# Effect of elastic strain energy on grain growth and texture in AZ31 magnesium alloy by phase-field simulation*

Ri He(何日), Ming-Tao Wang(王明涛)†, Jian-Feng Jin(金剑锋), and Ya-Ping Zong(宗亚平)

*School of Materials and Engineering & Key Laboratory for Anisotropy and Texture of Materials (Ministry of Education), Northeastern University, Shenyang* 110089, *China*

(Received 15 May 2017; revised manuscript received 18 July 2017; published online 20 October 2017)

A phase-field model is modified to investigate the grain growth and texture evolution in AZ31 magnesium alloy during stressing at elevated temperatures. The order parameters are defined to represent a physical variable of grain orientation in terms of three angles in spatial coordinates so that the grain volume of different order parameters can be used to indicate the texture of the alloy. The stiffness tensors for different grains are different because of elastic anisotropy of the magnesium lattice. The tensor is defined by transforming the standard stiffness tensor according to the angle between the (0001) plane of a grain and the direction of applied stress. Therefore, different grains contribute to different amounts of work under applied stress. The simulation results are well-explained by using the limited experimental data available, and the texture results are in good agreement with the experimental observations. The simulation results reveal that the applied stress strongly influences AZ31 alloy grain growth and that the grain-growth rate increases with the applied stress increasing, particularly when the stress is less than 400 MPa. A parameter ($\Delta d$) is introduced to characterize the degree of grain-size variation due to abnormal grain growth; the $\Delta d$ increases with applied stress increasing and becomes considerably large only when the stress is greater than 800 MPa. Moreover, the applied stress also results in an intensive texture of the $\langle 0001 \rangle$ axis parallel to the direction of compressive stress in AZ31 alloy after growing at elevated temperatures, only when the applied stress is greater than 500 MPa.

**Keywords:** phase-field simulation, elastic energy, texture, magnesium alloy

**PACS:** 82.20.Wt, 91.60.Ed, 81.40.Jj, 68.55.jm **DOI:** 10.1088/1674-1056/26/12/128201

## 1. Introduction

Magnesium alloys, the lightest metallic structural materials, have attracted significant attention in automotive and aerospace industries. However, because of the presence of limited slip systems stemming from their hexagonal close-packed structures, magnesium alloys exhibit relatively low strength and poor plasticity at room temperature; these shortcomings restrict their range of applications as engineering materials.[1–3] One of the most effective methods to improve their properties is to modify their microstructures, such as grain sizes, morphologies, or textures.[4–6]

Crystallographic texture is known as a main source of polycrystalline material plastic strain anisotropy and influences most of the mechanical, physical, and chemical properties of polycrystalline materials.[7–13] In the case of AZ31 magnesium alloy, the hot-rolled AZ31 magnesium alloy exhibits a strong basal texture with the $\langle 0001 \rangle$ axis parallel to the normal direction,[7,11] whereas the hot-extruded AZ31 magnesium alloy exhibits fiber texture with the $\langle 0001 \rangle$ axis parallel to the radial direction.[9] There are many reports that a random polycrystalline aggregate will develop a preferred orientation or texture upon sufficient plastic deformation. However, the resulting texture may be affected to some extent by the elastic strain energy and the phenomenon has not been recognized universally, probably because the texture measurement is difficult to identify which effect to determine a texture to what extent. Computer simulation has shown a promising significance to find processing reference parameters in order to control the texture of real industry alloys.[12,14,15]

The phase-field method is a physical and mathematical model used to predict microstructure evolution phenomena and offers unique advantages in studying the effect of applied stress on the microstructural evolution of alloy.[16] For instance, Wen *et al.*[17] used the phase-field method to investigate the effect of an applied homogeneous strain on the coherent $\alpha_2$ to $O$-phase transformation in Ti–Al–Nb alloys. Guo *et al.*[18] used the phase-field model to study the effect of a superimposed stress on the coarsening of interacting $Ni_4Ti_3$ particles. Recently, several researchers have studied the effect of strain on texture evolution by using the phase-field method. Kim *et al.*[19] established a phase-field model combined with a micro-elasticity effect including elastic anisotropy and inhomogeneity to investigate the effects of micro-elasticity on grain growth and texture evolution in polycrystalline thin film with columnar grain structure. Darvishi Kamachali *et al.*[20] proposed a phase-field model that used the contribution of

*Project supported by the National Key Research Development Program of China (Grant No. 2016YFB0701204) and the National Natural Science Foundation of China (Grant Nos. U1302272 and 51571055).

†Corresponding author. E-mail: wangmingtao@mail.neu.edu.cn

© 2017 Chinese Physical Society and IOP Publishing Ltd 

stored mechanical energy to investigate texture evolution in deformed AZ31 magnesium alloy sheets. Bahattacharyya *et al.*[21] developed the phase-field method integrated with a crystal plasticity effect to investigate the stress-driven grain-boundary migration in elastically inhomogeneous polycrystalline materials. Lu *et al.*[22] used the phase field method to study the effect of the second phase particle on texture evolution of polycrystalline material based on Bahattacharyya's work. However, the studies of influences of elastic strain energy on texture evolution and grain growth by the phase-field method are not found in the literature probably because it is generally believed that texture and grain growth at high temperature are determined by anisotropic plastic strain in terms of stored energy only, and features of elastic strain energy have no effect.[12] The aim of this simulation is to prove the possibility that anisotropic elastic strain energy plays an important role in texture formation as well during grain growth under applied stress. This model works on the assumption that the stored energy is immediately released in the case that AZ31 alloy is deformed slowly with temperature increasing. Our previous work already established a phase-field model which takes the contribution of stored energy into consideration to simulate the grain growth process of AZ31 alloy in real time and space by introducing a novel concept of the grain boundary range.[23–26]

In this study, we develop a phase-field model to investigate the influences of elastic strain energy on grain growth and texture by setting no plastic strains in AZ31 Mg alloy. The order parameters are defined to represent a physical variable of grain orientation so that elastic energy and texture can be expressed by analytical formulas. The anisotropic elastic energy in grain as an extra grain growth driving force is calculated in the present work under applied stress and is different among grains due to different angles of grain orientation with respect to the applied stress direction. The simulation results are explained by using the experimental data. This work will provide a new general theoretical guideline for developing the industrial magnesium alloys.

## 2. Model description

Phase-field methods are based on classical thermodynamics and kinetics theory. The phase-field model uses a set of field variables (e.g., concentration field variable and order parameters) to simulate complex microstructures. The temporal evolution of the microstructure can be determined by solving the time-dependent Ginzburg–Landau equation[27] and the Cahn–Hilliard diffusion equation[28] as follows:

$$\frac{\partial \eta_p(r,t)}{\partial t} = -L\frac{\delta F}{\delta \eta_p(r,t)}, \quad p = 1,2,3,\ldots,n, \tag{1}$$

$$\frac{\partial c(r,t)}{\partial t} = M\nabla^2\frac{\delta F}{\delta c(r,t)}, \tag{2}$$

where $L$ is the interface mobility, $F$ is the free energy of the system, $M$ is the chemical diffusion mobility, $\eta_p(r,t)$ represents the long-range order parameters, and $c(r,t)$ is a concentration field variable. The long-range order parameters represent the different crystallographic orientations of grains.

The free energy of the system $F$ is expressed as a function of the chemical free energy $F_{\rm ch}$ and the elastic free energy $E_{\rm el}$ as follows:

$$F = F_{\rm ch} + E_{\rm el}. \tag{3}$$

The concentration field variable is dependent on the order parameter at any position; i.e., the gradient form of concentration is a function of the gradient form of the order parameter. It is equivalent to choose any of the gradient forms as zero and we choose the concentration to be zero as in previous work.[29] Therefore, the single-phase system chemical free energy is typically expressed as

$$F_{\rm ch} = \int \left[\frac{1}{2}K_2\sum_{p=1}^{n}(\nabla\eta_p)^2 + f_0(c(r,t),\eta_1,\eta_2.\eta_n)\right]{\rm d}^3r, \tag{4}$$

where $f_0$ is the local free energy density function and $K_2$ is the gradient energy coefficient.

In the present study, based on the work of Wu *et al.*[25] and He *et al.*,[26] the following expression is introduced to describe the free energy density function:

$$\begin{aligned} f_0 =\ & A + A_1(c(r,t)-c_l)^2 + \frac{A_2}{4}(c(r,t)-c_l)^4 \\ & - \frac{B_1}{2}(c(r,t)-c_l)^2\sum_{p=1}^{n}\eta_p^2(r,t) + \frac{B_2}{4}\left(\sum_{p=1}^{n}\eta_p^2(r,t)\right)^2 \\ & + \frac{K_1}{2}\sum_{p=1}^{n}\sum_{p\neq q}^{n}\eta_p^2(r,t)\eta_q^2(r,t), \end{aligned} \tag{5}$$

where $c(r,t)$ is the concentration of all elements in the $\alpha$-Mg matrix. However, the concentration of Zn elements is very low compared with that of Al and its variation contributes very little to the total free energy; therefore, for simplicity, we only calculate the Al concentration, so that $c(r,t)$ is the Al concentration, i.e., the AZ31 is simplified into Mg–3Al alloy, $c_l$ is the Al concentration at the lowest point of the free energy curve as a function of temperature, and $K_1$ is the coefficient of coupling between $\eta_p$ and $\eta_q$.

On the basis of the linear elasticity theory introduced by Khachaturyan,[30] the elastic energy of a homogeneous anisotropic system can be expressed as a function of $\eta_p(r,t)$ as follows:

$$\begin{aligned} E_{\rm el} =\ & \frac{V}{2}C_{ijkl}\bar{\varepsilon}_{ij}\bar{\varepsilon}_{kl} - VC_{ijkl}\bar{\varepsilon}_{ij}\sum_p\varepsilon_{kl}^0(p)\overline{\eta_p^2(r,t)} \\ & + \frac{V}{2}C_{ijkl}\sum_p\sum_q\varepsilon_{ij}^0(p)\varepsilon_{kl}^0(q)\overline{\eta_p^2(r,t)\eta_q^2(r,t)} \end{aligned}$$

$$-\frac{1}{2}\sum_{p}\sum_{q}\int\frac{d\vec{g}}{(2\pi)}B_{pq}(n)\left\{\eta_p^2(r,t)\right\}_g^*\left\{\eta_q^2(r,t)\right\}_g, \quad (6)$$

where $V$ is the total volume of the system, $C_{ijkl}$ is the elastic constant tensor, $\overline{(\cdots)}$ represents the volume average of $(\cdots)$, $\varepsilon_{ij}^0(p)$ is the eigenstrain for the $p$-th orientation, and $\overline{\varepsilon_{ij}}$ is the elastic strain. Parameter $B_{pq}(n)$ is a two-body elastic interaction potential and is given by

$$B_{pq}(\boldsymbol{n}) = n_i\sigma_{ij}^0(p)\Omega_{jk}(\boldsymbol{n})\sigma_{kl}^0(q)n_l, \quad (7)$$

$$\Omega_{ij}^{-1}(\boldsymbol{n}) = C_{ijkl}n_k n_l, \quad (8)$$

where $n = \boldsymbol{g}/g$ is a unit vector in reciprocal space and $n_p$ is its $p$-th grain orientation, $\left\{\eta_q^2(\boldsymbol{r})\right\}_g$ is the Fourier transform of $\eta_q^2(\boldsymbol{r})$, and $\left\{\eta_p^2(\boldsymbol{r})\right\}_g^*$ is the complex conjugate of $\left\{\eta_q^2(\boldsymbol{r})\right\}_g$.

In this model, the same stress is applied to all grains, but the strain is different according to the different orientation of grains. The elastic inhomogeneity could result in different eigenstrains for different grains according to the linear elasticity theory proposed by Khachaturyan.[30] Therefore, the eigenstrain is coupled to generate elastic energy by the 3rd term as well as a relaxation that affects each other in the 4th term. Actually, it can be traced back to Eshelby's classical work on transformation-induced elasticity,[31] this strain comes from the mismatch strain. The eigenstrain tensor of each orientation is obtained by transforming the constant tensor with respect to the crystal coordinate system of $x = [10\bar{1}0]$, $y = [\bar{1}2\bar{1}0]$, and $z = [0001]$, and given by

$$\varepsilon_{ij}^0(p) = \sum_p a_{ip}^p a_{jq}^p a_{kr}^p a_{ls}^p \varepsilon_{ij}^*, \quad (9)$$

where $\varepsilon_{ij}^*$ is a constant tensor, which is determined by the coordinate system of applied stress, and is expressed as follows:

$$\varepsilon_{ij}^* = \begin{pmatrix} -1/2 & \sqrt{3}/2 & 0 \\ \sqrt{3}/2 & 1/2 & 0 \\ 0 & 0 & 0 \end{pmatrix}, \quad (10)$$

and $a$ is the transformation matrix representing the rotation of the coordinate system defined on a given grain $p$ with respect to the fixed reference coordinate, which is expressed in terms of three Euler angles $\varphi_1$, $\Phi$, and $\varphi_2$ as follows:

$$a_{ij}^p = \begin{pmatrix} \cos\varphi_1\cos\varphi_2 - \sin\varphi_1\sin\varphi_2\cos\Phi & \cos\varphi_1\cos\varphi_2 + \sin\varphi_1\sin\varphi_2\cos\Phi & \sin\varphi_2\sin\Phi \\ -\cos\varphi_1\sin\varphi_2 - \sin\varphi_1\cos\varphi_2\cos\Phi & -\sin\varphi_1\sin\varphi_2 + \cos\varphi_1\cos\varphi_2\cos\Phi & \cos\varphi_2\sin\Phi \\ \sin\varphi_1\sin\Phi & -\cos\varphi_1\sin\Phi & \cos\Phi \end{pmatrix}, \quad (11)$$

with $0 \le \varphi_1 \le 2\pi$, $0 \le \Phi \le \pi$, and $0 \le \varphi_2 \le 2\pi$.

Each orientation is represented by the three Euler angles $\varphi_1$, $\Phi$, and $\varphi_2$, and each order parameter $\eta p(r,t)$ is defined to represent a physical variable of the grain orientation as shown in Table 1. The elastic constants of the AZ31 alloy used in this simulation are $C_{11} = 65.6$ GPa, $C_{12} = 25.9$ GPa, $C_{13} = 19.3$ GPa, $C_{33} = 69.0$ GPa, $C_{44} = 13.6$ GPa, and $C_{66} = 19.85$ GPa.[32]

**Table 1.** Corresponding relationship between order Parameters and Euler angles.

| Order parameter ($\eta_p$) | $\varphi_1/(^\circ)$ | $\Phi/(^\circ)$ | $\varphi_2/(^\circ)$ |
|---|---|---|---|
| $\eta_1$ | 0 | 0 | 0 |
| $\eta_2$ | 10 | 5 | 10 |
| $\eta_3$ | 20 | 10 | 20 |
| ⋮ | ⋮ | ⋮ | ⋮ |
| $\eta_{35}$ | 340 | 170 | 340 |
| $\eta_{36}$ | 350 | 175 | 350 |

This simulation investigates the elastic strain energy effect via a mock situation where the AZ31 alloy is deformed slowly at an elevated temperature that was sufficiently high to immediately relieve the stored energy in dislocation annihilation by means of dislocation climbing. Therefore, it is believed that plastic strain has a minor effect in this particular case.[33] The parameters related to the chemical free energy in Eqs. (4) and (5) are determined by physical analysis or experimental data from real AZ31 alloy, and we use the method described in our recent studies to obtain the parameters values.[24–26] The results of the present simulation indicate that the grain boundary range should properly take a value of 1.2 μm for consistency with the experimental results; therefore, $K_2$ must take a value of $3.0\times10^{-12}$ J·m$^2$·mol$^{-1}$ according to our simulations. Both $K_1$ and $K_2$ substantially affect grain boundary energy determined by simulation. The random grain boundary energy is measured to be between 0.5 J·m$^{-2}$ and 0.6 J·m$^{-2}$ for most previously investigated polycrystalline metal systems; thus, here, 0.55 J·m$^{-2}$ is set to be the target value. By our simulation, we determine that $K_1 = 4.0\times10^{-2}$ J·mol$^{-1}$ if the calculated boundary energy satisfies a target value. The diffusion mobility $M$ in Eq. (2) is approximately $3.87\times10^{-20}$ m$^2$·mol·J$^{-1}$·s$^{-1}$ according to Ref. [34] because the process of grain growth involves no long-range transport of atoms and is an interface controlled transformation where the $M$ value does not play an important role. The $c_l$ is taken as 0.2 at temperature in a range from 573K to 673 K according to the experimental energy concentration curve.[24] The values of all the necessary parameters for the present model are summarized in Table 2. Furthermore, all grain boundaries are assumed to be random high-angle boundaries, and it is considered as a good approximation for general metals in elevated-temperature grain growth.

**Table 2.** Values of model parameters at different temperatures.

| Temperature/K | $A$/kJ·mol$^{-1}$ | $A_1$/kJ·mol$^{-1}$ | $A_2$/kJ·mol$^{-1}$ | $B_1$/J·mol$^{-1}$ | $B_2$/J·mol$^{-1}$ | $K_1\times10^{-2}$/J·mol$^{-1}$ | $K_2\times10^{-12}$/J·m$^2$·mol$^{-1}$ | $L\times10^{-7}$/m$^2$·mol·J$^{-1}$s$^{-1}$ |
|---|---|---|---|---|---|---|---|---|
| 573 | −19.5 | 22.1 | 5.2 | 106.12 | 3414 | 4.0 | 3.0 | 0.61 |
| 623 | −22.1 | 22.5 | 13.0 | 106.12 | 3414 | 4.0 | 3.0 | 1.12 |
| 673 | −25.0 | 22.0 | 18.3 | 106.12 | 3414 | 4.0 | 3.0 | 1.72 |

The simulations are performed in a two-dimensional (2D) grid size of $1024^2$ cells. A three-dimensional (3D) simulation is also carried out for comparison with the 2D simulation; the 3D size is $512^3$ grid cells. Each grid cell is 0.1 μm in size and the time step value is selected as 0.2 s in this model to maintain a balance between convergence and efficiency. The periodic boundary condition is imposed. The initial microstructure is defined as an average grain size of 11 μm with grains being in randomly different crystallographic orientations. The initial Al concentration is set to be a different value according to the local initial $\eta$ value. If $\eta = 1$, the local initial concentration is set to be 0.03, and at other positions it is set to be 0.031 for simulating the element boundary segregation. This simulation uses the semi-implicit Fourier-spectral method to solve the model Eqs. (1) and (2), and we have used the same technique in our previous work,[35] which is described in detail in Ref. [36].

## 3. Results and discussion

The simulation is performed in both 2D and 3D cases to investigate the effects of an applied stress of 400-MPa on the grain growth in polycrystalline AZ31 Mg alloy. In the case of the 2D simulation, the microstructure after the alloy has been annealed at 673 K for 60 min is shown in Fig. 1(a), and the average grain sizes versus annealing time with and without stress are shown as curve 1 and curve 2 in Fig. 2, respectively. In the case of the 3D simulation, the alloy microstructure is shown in Fig. 1(b) and the cross-sectional 3D view is shown in Fig. 1(c). The grain sizes versus annealing time in 3D simulations with and without stress are statistically obtained by averaging the sphere diameters of grains, as determined from their volumes; the results are shown in Fig. 2 as curve 3 and curve 4, respectively.

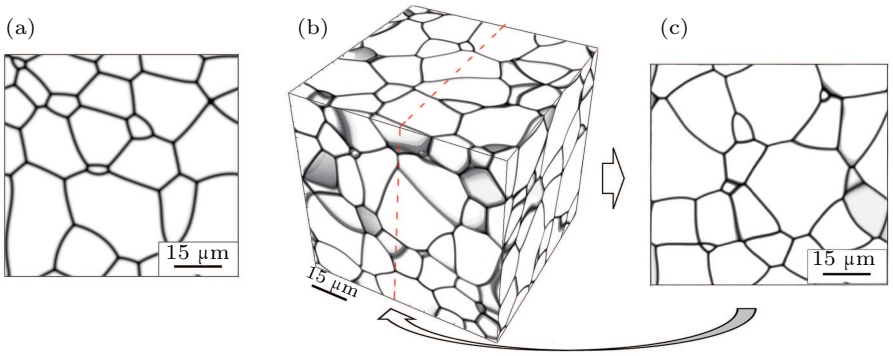



**Fig. 1.** (color online) Comparison between simulated grain growths using (a) two- and (b) three-dimensional models for AZ31 alloy annealed under an applied stress of 400 MPa for 60 min at 673 K, and (c) cross-sectional view at the red dotted line shown in panel (b) (i.e., a three-dimensional model expressed in two dimensions).

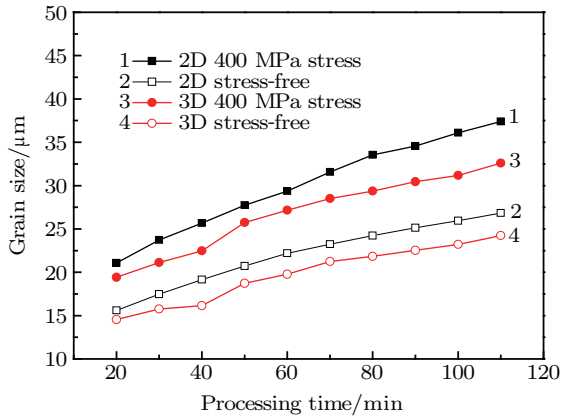



**Fig. 2.** (color online) Grain growths in AZ31 magnesium alloy as a function of annealing time, predicted by the two- and three-dimensional simulations of AZ31 magnesium alloy annealed with and without applied stress at 673 K.

A comparison between the 2D and 3D simulation results in Fig. 1 reveals that the 2D and cross-sectional 3D morphologies are similar. Figure 2 shows that for both simulations under the condition without and with stress, the trends of grain-growth rate increasing with the increase of applied stress are in the same manner. The 3D simulations differ substantially from 2D simulations and cannot be substituted by 2D simulations in systems of anisotropic interface energy and mobility. However, our model shows the effect of elastic strain energy on the grain growth rate in a general isotropic system, and this study intends to find a new general theoretical reference for developing the industrial magnesium alloys rather than specific datum finding. We find that our 2D simulation provides satisfactory results. To improve the calculation efficiency, we use 2D simulations in the rest of this work; thus, all simulations

hereafter are 2D.

In this study, we investigate the effects of different applied stress values on the grain growth in polycrystalline AZ31 alloy. The direction of stress is crucial, indeed if local behavior and morphology are chiefly concerned. However, the direction of stress is isotropic in an enormous system of randomly oriented grains. We arbitrarily choose a stress direction parallel to the $z$ axis for convenience. The evolutions of the microstructures during grain growth under different applied compressive stresses are plotted in Fig. 3. It is found that the grains are fine and uniform in the stress-free condition, whereas grain coarsening occurs under applied stress; extra-large grains appear when the stress is 1000 MPa.

In order to quantitatively investigate the variation of average grain size, we simulate the variations of grain size with annealing time under different applied stresses. Figure 4 shows a plot of the changes of average grain size with increasing annealing time under different applied stresses at 673 K. The results show that the grain-growth rate in AZ31 alloy increases with applied stress increasing. Compared with the sample prepared without applied stress, the sample annealed for 100 min under an applied stress of 200 MPa increases the average grain size by 22.6%. In addition, when the stress is greater than 400 MPa, any further increase of stress negligibly affects the average grain size.

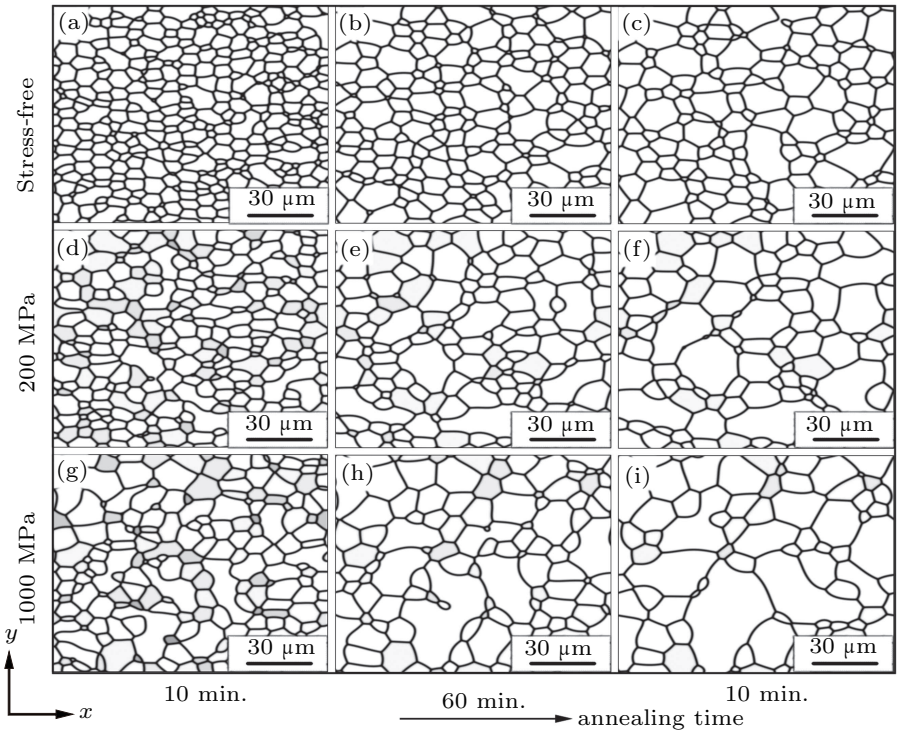



**Fig. 3.** Grain growths in AZ31 alloy under different applied stresses: (a)–(c) without applied stress, (d)–(e) under an applied stress of 200 MPa, and (g)–(i) under an applied stress of 1000 MPa, respectively. Each column represents different annealing times from 10 min to 100 min.

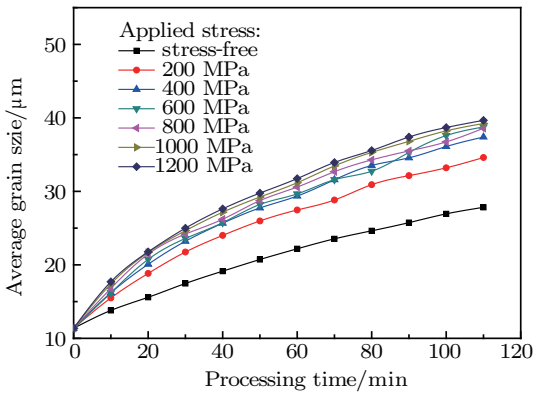



**Fig. 4.** (color online) Plots of average grain size of AZ31 magnesium alloy as a function of annealing time under different applied stresses at 673 K, determined by simulation.

The distributions of grain size in AZ31 alloy annealed for 100 min under several different applied stresses are shown in Fig. 5. The changes in the distributions show that the number of small grains (grain size $\leq$ 20 μm) decreases and the number of large grains (grain size $\geq$ 50 μm) increases with applied stress increasing as revealed by a comparison between Figs. 5(a) and 5(b). However, the number of small grains remains almost unchanged when the applied stress increases from 600 MPa to 1200 MPa. We observe that extra-large grains appear under an applied stress of 1200 MPa, possibly because stress produces different levels of elastic energy in grains as a result of different grain orientations, and a grain with high elastic energy may shrink quickly resulting in abnormal grain growth at its neighbor. This demonstrates that the applied stress enhances the grain growth kinetic property and may lead to the abnormal growth of grain.

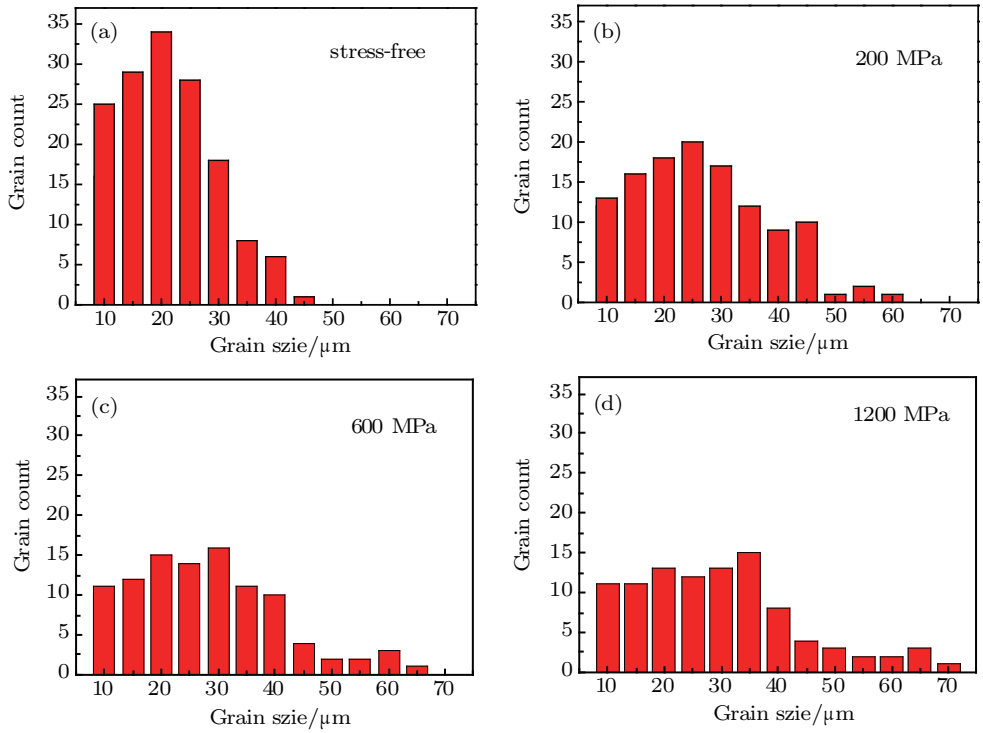



**Fig. 5.** (color online) Grain size distributions of AZ31 magnesium alloy grown for 100 min at 673 K under different applied stresses: (a) stress-free, (b) 200-MPa applied stress, (c) 600-MPa applied stress, and (d) 1200-MPa applied stress.

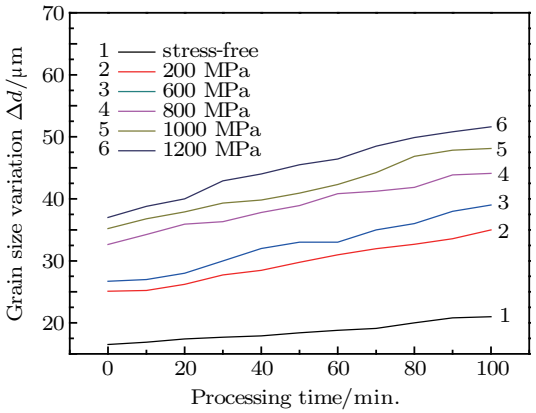



**Fig. 6.** (color online) Plots of simulated grain size variation ($\Delta d$) as a function of the annealing time for growth at 673 K under different applied stresses.

To obtain an accurate expression for grain-size variation, we introduce a parameter $\Delta d$ to describe it: $\Delta d = d_{\max} - d_{\min}$, where $d_{\max}$ represents the maximal characteristic grain size, which is the average size of the 10% of the largest grains in a system, and $d_{\min}$ is the minimal characteristic grain size, which is the average size of the 10% of the smallest grains. The simulated grain-size variations with processing time are plotted in Fig. 6 for various applied stresses. Notably, the grain-size variations shown here are not the deviations of the grain size from the corresponding value in the common normal distribution of the grain size. The variation here is used to represent the degree of grain size fluctuation due to abnormal grain growth. Figure 6 shows that grain-size fluctuation increases with processing time and applied stress increasing. However, grain-size fluctuation becomes severe when the applied stress is greater than 800 MPa; it suggests that abnormal grain growth depends on the applied stress field to some extent. This phenomenon has rarely been reported in similar modeling studies.

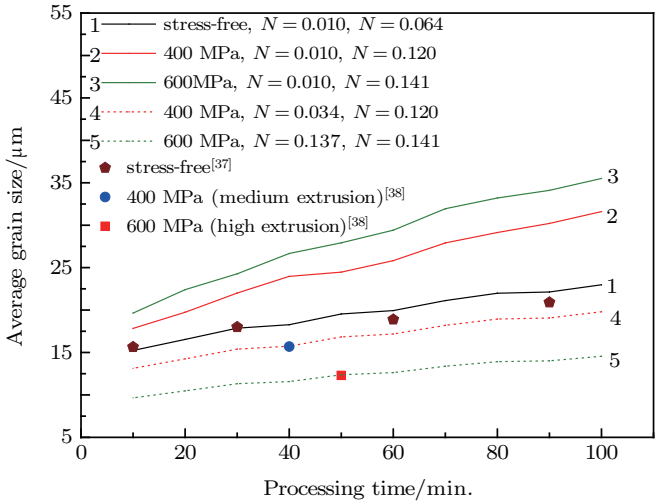



**Fig. 7.** (color online) Simulated grain growth in AZ31 alloy with and without applied stress for comparison with experiments at 623 K:[37,38] curves 1, 2, and 3 are simulations at a nucleation rate of 0.010, obtained by our model setup, and the growth rates are different obtained by fitting the simulation data to Eq. (12); curves 2 and 3 become curves 4 and 5 respectively if the nucleation rate is varied accordingly.

In this work, we simulate grain growth under applied stress on an industrial application scale. It is necessary to explore the significance of applied stress in industrial applications. Figure 7 shows a comparison between the simu-

lated grain growths of AZ31 magnesium alloy with and without applied stress with experimental data at 623 K.[37,38] The medium extrusion in experiment corresponds to 400 MPa and high extrusion corresponds to 600 MPa approximately.[38] The grain size by experiment as a function of plastic strain at elevated temperature is believed to be equivalent to one as a function of time and the applied stress level given by the experiment, so that it is suggested that there is a 10-min difference between medium extrusion and high extrusion.

Figure 7 shows that better agreement is achieved between the simulation and experiment under the stress-free condition but simulations contradict the experiment under applied stress and the stress reduces the average grain size, which phenomenon is in contrast to the experimental fact. We try to use the Johnson–Mehl equation to explain that discrepancy. The Johnson–Mehl equation[39] gives a correlation between the grain size ($d$), nucleation rate ($\dot{N}$), and grain-growth rate ($G$) as

$$d = k\left(\frac{G}{\dot{N}}\right)^{1/4}, \tag{12}$$

where $k$ is a constant that depends on the grain-growth time. It is assumed that the grain-growth kinetics of AZ31 alloy follows the conventional kinetic Johnson–Mehl equation. The $\dot{N}$ is a small constant value of approximately 0.010/μm$^2$·min in our model setup, and we cannot set a larger $\dot{N}$ value so far due to our model capability. Therefore, different values of $G$ are obtained when the simulation data are applied in Eq. (12) as shown in the legend of Fig. 7. According to the conventional Johnson–Mehl kinetics described in Eq. (12), if the values of $\dot{N}$ take 0.034 and 0.137/μm$^2$·min and the growth rates are the values predicted by our simulation, then the simulation results can be revised, i.e., curve 2 becomes curve 4, and curve 3 becomes curve 5. The values of $k$ in Eq. (12) at any time can be calculated by using the data of any curve in Fig. 7 and the obtained values are listed in Table 3. This work on the nucleation is only a numerical fit based on Eq. (12), so that nucleation plays an important role but nucleation is not necessarily caused by elastic energy rather by plastic straining in the experiment.

**Table 3.** Values of $k$ at different growth times in Eq. (12), determined by fitting the data corresponding to curve 1 in Fig. 7.

| Time/min. | 10 | 20 | 30 | 40 | 50 | 60 | 70 | 80 | 90 | 100 |
|---|---|---|---|---|---|---|---|---|---|---|
| $k$/μm$^{1/4}$ | 9.58 | 10.40 | 11.23 | 11.49 | 12.29 | 12.54 | 13.28 | 13.82 | 13.91 | 14.45 |

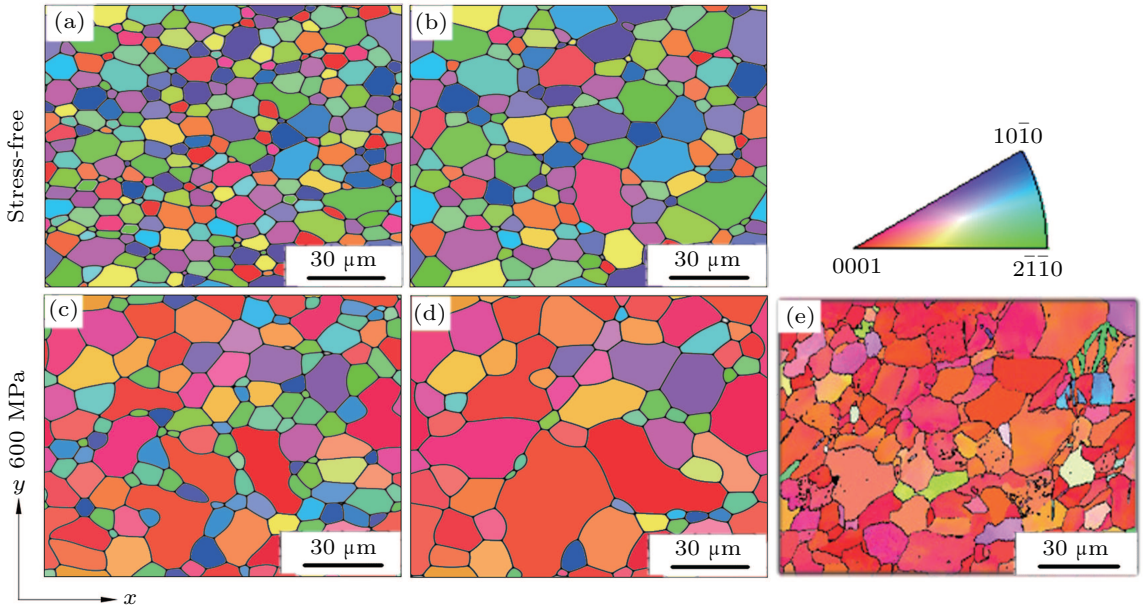



**Fig. 8.** (color online) Simulated texture of AZ31 alloy after being annealed at 673 K for 40 min and 100 min with and without applied stress: (a) and (b) stress-free, (c)–(d) under 600 MPa applied stress, and (e) EBSD experimental texture corresponding to AZ31 samples dynamically loaded at 523 K in compression along the normal direction to a strain of 0.17.[40]

The AZ31 specimen of our simulation is compressed at 673 K. The direction of compressive stress is along the $z$ axis in space coordinate. In the simulation, texture evolution starts with the same initial random texture microstructure. Figure 8 shows the texture of AZ31 alloy after being annealed at 673 K for 40 min and 100 min with and without applied stress. The texture is expressed as an orientation color map in which red, blue, and green represent the hexagonal $\langle 0001\rangle$, $\langle 10\bar{1}0\rangle$, and $\langle 2\bar{1}\bar{1}0\rangle$ direction parallel to the $z$ axis, respectively. Figures 8(a) and 8(b) show that the polycrystalline AZ31 alloy remains randomly orientated but grain size increases during annealing with stress-free, because the normal grain growth is determined by curvature-driven grain boundary migration. Figures 8(c) and 8(d) show that applied stress enhances the growths of grains with special orientations. The initial random texture changes into a strong $\langle 0001\rangle$ texture, whereas un-

favorable textures of $\langle 10\bar{1}0\rangle$ and $\langle 2\bar{1}\bar{1}0\rangle$ decrease dramatically under applied stress. Dudamell *et al.* reported a similar result for an AZ31 alloy sample deformed under compression along the normal direction, where the basal texture of the $\langle 0001\rangle$ axis parallel to the normal direction appears with increasing deformation as shown in Fig. 8(e).[40] Darvishi Kamachali *et al.*[20] also proposed a phase field model to study the texture evolution in AZ31 alloy, they found that during annealing of deformed AZ31 sheets, the inhomogeneous stored mechanical energy leads to the preferential formation of a $\{2\bar{1}\bar{1}0\}$ texture. Our simulation indicates that a $\langle 0001\rangle$ dynamic recrystallization texture is formed by grain growth under stress without stored energy due to elastic inhomogeneity. This suggests that the anisotropies of elastic strain energy and stored mechanical energy affect the formation of texture but the extent and type of the texture are different.

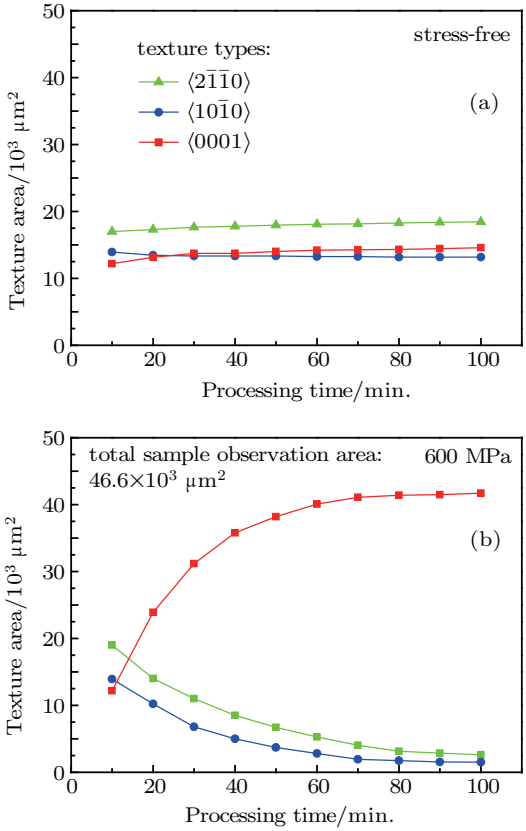



**Fig. 9.** (color online) Texture evolutions upon grain growth in AZ31 alloy with and without applied stress: (a) without applied stress and (b) 600 MPa applied stress.

In order to better understand texture evolution, we quantitatively study the variation of the texture area. Figure 9(a) shows the evolutions of three types of textures ($\langle 0001\rangle$, $\langle 10\bar{1}0\rangle$, and $\langle 2\bar{1}\bar{1}0\rangle$) during 100-min annealing under the stress-free condition. The total sample observation area of the three textures is $46.6\times10^3$ μm$^2$. The results show that during grain growth, the texture area exhibits almost no change with stress-free. It is found in Fig. 9(b) that the texture area changes under an applied stress of 600 MPa and the evolution of texture is significantly affected, in which the texture of $\langle 0001\rangle$ grows preferentially from $12.3\times10^3$ μm$^2$ to $41.7\times10^3$ μm$^2$, whereas the textures of $\langle 10\bar{1}0\rangle$ and $\langle 2\bar{1}\bar{1}0\rangle$ decrease significantly, which is probably because elastic-energy driven is more dominant than boundary curvature-driven in grain boundary migration at this stage. In addition, the simulation examines the effects of different applied stresses on texture evolution; we observe that the applied stress results in an intensive recrystallization texture only when it is greater than 500 MPa.

The topological structure is a particularly important characteristic in polycrystalline alloy, it will play a key role in grain-growth dynamics. Therefore, it is necessary to investigate the topological evolution of each individual grain during growth and shrinkage.

Note that von Neumann and Mullins gave a correlation between the growth rate of $n$-sided grain in two dimensions and the topological class of each individual grain under the stress-free condition:[41]

$$\frac{\mathrm{d}A}{\mathrm{d}t}=\frac{\pi M\sigma}{3}(n-6), \tag{13}$$

where $A$ is the grain area, $M$ is the mobility, and $\sigma$ is the grain-boundary energy. According to Eq. (13), a grain with $n>6$ will grow, whereas a grain with $n<6$ will shrink. Figures 10(a)–10(c) show an example of in situ observation of four types of topological transformations during simulating grain evolution under the stress-free condition. Grain A with $n=7$ and grain D with $n=9$ are observed to grow, whereas grain B with $n=4$ and grain C with $n=5$ are observed to shrink and later disappear; this is consistent with the von Neumann–Mullins grain-growth law. In addition, we observe that grain C with five sides transforms into a four-sided grain and then disappears, and that $n$ of grain A remains unchanged during the grain growth under the stress-free condition.

Figures 10(d)–10(f) show topological changes of grains with the same initial microstructure under an applied stress of 600 MPa; it can be seen that grain A with $n=7$ and grain B with $n=4$ are shrinking, whereas grain C with $n=5$ and grain D with $n=9$ are growing. These results illustrate that the grain growth under applied stress is not consistent with the von Neumann–Mullins grain-growth law. Moreover, we observe that the 5-sided grain C is transformed into a 6-sided grain during grain growth and that the 7-sided grain A is transformed into a 3-sided grain under an applied stress of 600 MPa. Interestingly, under applied stress, we observe that some of the preferred orientation grains, such as grain C, are growing and that the grain boundaries have developed a negative curvature even if they are small and their neighbors are larger. This behavior is likely to be attributable to the grains favorably oriented with respect to the direction of applied stress.

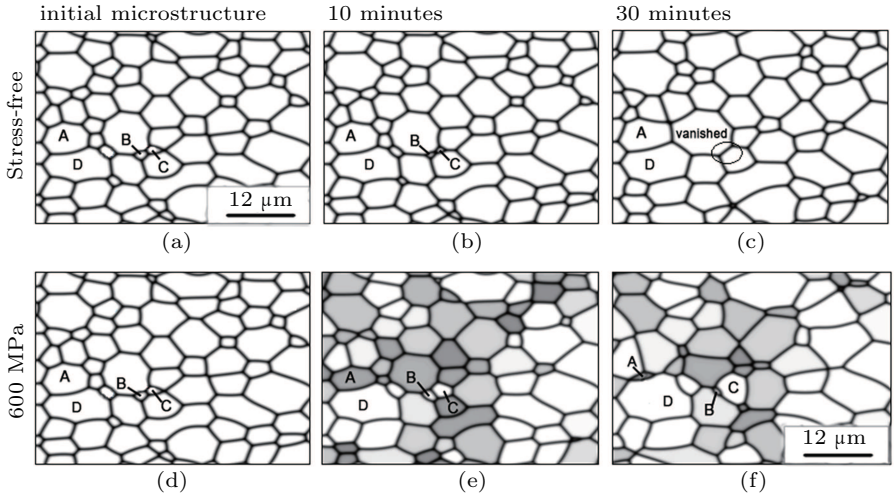



**Fig. 10.** Topological evolutions of microstructure under (a)–(c) no stress and (d)–(f) 600 MPa applied stress to demonstrate some topological transformation features at 673K during annealing time.

This phase-field model is established to simulate the effects of applied stress on grain growth and texture in polycrystalline AZ31 alloy. Moreover, this model is sufficiently flexible to be adapted to simulating other alloy systems under applied stress by changing the value of the dynamic parameters and the expression of $f_0$.

## 4. Conclusions

(i) A phase-field model is modified to simulate grain growth and texture evolution in AZ31 magnesium alloy at elevated temperatures under an applied stress field by determining different stiffness tensors for each grain orientation with respect to the direction of applied stress. The texture results exhibit good agreement with the experimental observation.

(ii) Applied stress strongly influences grain growth in AZ31 alloy at elevated temperature, and the grain-growth rate increases with applied stress increasing, particularly when the applied stress is less than 400 MPa.

(iii) A parameter ($\Delta d$) is introduced to show the degree of grain size variation due to abnormal grain growth and the $\Delta d$ increases with increasing applied stress. The $\Delta d$ becomes severely large only when the stress is greater than 800 MPa.

(iv) Applied stress would result in an intensive texture of $\langle 0001 \rangle$ along the compressive stress direction in AZ31 alloy grown at elevated temperature only when the applied stress is greater than 500 MPa.

## References


[1] Tang Y and El-Awady J A 2014 *Acta Mater.* **71** 319
[2] Zhang J and Joshi S P 2012 *J. Mech. Phys. Solids* **60** 945
[3] Agnew S R and Duygulu Ö 2005 *Int. J. Plast.* **21** 1161
[4] Kim W J, Lee Y G, Lee M J, Wang J Y and Park Y B 2011 *Scr. Mater.* **65** 1105
[5] Yin S M, Wang C H, Diao Y D, Wu S D and Li S X 2011 *J. Mater. Sci. Technol.* **27** 29
[6] del Valle J A, Carreño F and Ruano O A 2006 *Acta Mater.* **54** 4247
[7] Victoria-Hernandez J, Yi S, Bohlen J, Kurz G and Letzig D 2014 *J. Alloys Compd.* **616** 189
[8] Chai S, Zhang D, Pan F, Dong J, Guo F and Dong Y 2013 *Mater. Sci. Eng. A* **588** 208
[9] Laser T, Hartig C, Nürnberg M R, Letzig D and Bormann R 2008 *Acta Mater.* **56** 2791
[10] del Valle J A and Ruano O A 2008 *Mater. Sci. Eng. A* **487** 473
[11] Kim S H, You B S, Dong Yim C and Seo Y M 2005 *Mater. Lett.* **59** 3876
[12] Suwas S and Ray R K 2014 *Crystallographic Texture of Materials* (London: Springer) pp. 108–137
[13] Lu L, Huang J W, Fan D, Bie B X, Sun T, Fezzaa K, Gong X L and Luo S N 2016 *Acta Mater.* **120** 86
[14] Chumachenko E N 2009 *Mater. Sci. Eng. A* **499** 342
[15] Ramakrishnan N and Ramarao P 1999 *Mater. Sci.* **22** 829
[16] Steinbach I 2009 *Modell. Simul. Mater. Sci. Eng.* **17** 073001
[17] Wen Y H, Wang Y and Chen L Q 2001 *Acta Mater.* **49** 13
[18] Guo W, Steinbach I, Somsen C and Eggeler G 2011 *Acta Mater.* **59** 3287
[19] Kim D U, Cha P R, Kim S G, Kim W T, Cho J, Han H N, Lee H J and Kim J 2012 *Comp. Mater. Sci.* **56** 58
[20] Darvishi Kamachali R, Kim S J and Steinbach I 2015 *Comp. Mater. Sci.* **104** 193
[21] Bhattacharyya S, Heo T W, Chang K and Chen L Q 2011 *Modell. Simul. Mater. Sci. Eng.* **19** 035002
[22] Lu Y L, Zhang L C, Zhou Y Y and Chen Z 2014 *Chin. Phys. B* **23** 069102
[23] Wang M T, Zong B Y and Wang G 2008 *J. Mater. Sci. Technol.* **24** 829
[24] Wang M T, Zong B Y and Wang G 2009 *Comp. Mater. Sci.* **45** 217
[25] Wu Y, Zong B Y, Zhang X G and Wang M T 2012 *Metall. Trans. A* **44** 1599
[26] He R, Wang M T, Zhang X and Zong B Y 2016 *Modell. Simul. Mater. Sci. Eng.* **24** 055017
[27] Allen S M and Cahn J W 1979 *Acta Met.* **27** 1085
[28] Cahn J W and Hilliard J E 1958 *J. Chem. Phys.* **28** 258
[29] Fan D and Chen L Q 1997 *Acta Mater.* **45** 611
[30] Khachaturyan A G 1983 *Theory of structure transformation in solids* (New York: John Wiley & Sons) pp. 198–212
[31] Eshelby J D 1957 *Proc. Roy. Soc. London* **241** 376
[32] Ganeshan S, Shang S L, Wang Y and Liu Z K 2009 *Acta Mater.* **57** 3876
[33] Nourollahi G A, Farahani M, Babakhani A and Mirjavadi S S 2013 *Mater. Res.* **16** 1309
[34] Moreau G, Cornet J A and Calais D 1971 *J. Nucl. Mater.* **38** 197
[35] Zhang X G, Wang M T, He R, Li W K and Zong B Y 2017 *Comp. Mater. Sci.* **127** 261
[36] Chen L Q and Shen J 1998 *Comput. Phys. Commun.* **108** 147
[37] Liu R C, Wang L Y, Gu L G and Huang G S 2004 *Light Alloy Fabric. Technol.* **23** 22
[38] Zhang X P, Castagne S, Luo X F and Gu C F 2011 *Mater. Sci. Eng. A* **528** 838
[39] Johnson W A and Mehl R F 1939 *Trans. Am. Inst. Min. Metall. Pet. Eng. Inc.* 416
[40] Dudamell N V, Ulacia I, Gálvez F, Yi S, Bohlen J, Letzig D, Hurtado I and Pérez-Prado M T 2012 *Mater. Sci. Eng. A* **532** 528
[41] Mullins W W 1956 *J. Appl. Phys.* **27** 900